

# $\Omega$ and biasing from optical galaxies versus POTENT mass

M.J. Hudson,<sup>1</sup> A. Dekel,<sup>2</sup> S. Courteau,<sup>3</sup> S.M. Faber<sup>4</sup> and J.A. Willick<sup>5</sup>

<sup>1</sup> Dept. of Physics, Univ. of Durham, South Road, Durham DH1 3LE. E-mail: M.J.Hudson@durham.ac.uk

<sup>2</sup> Racah Institute of Physics, The Hebrew University of Jerusalem, Jerusalem 91904, Israel. E-mail: dekel@vms.huji.ac.il

<sup>3</sup> Kitt Peak National Observatory, P.O. Box 26732, Tucson, AZ 85726-6732, USA. E-mail: courteau@noao.edu

<sup>4</sup> UCO/Lick Observatory, University of California, Santa Cruz, CA 95064, USA. E-mail: faber@lick.ucsc.edu

<sup>5</sup> Carnegie Observatories, 813 Santa Barbara St., Pasadena, CA 91101, USA. E-mail: jeffw@cetus.ociw.edu

Accepted 1995 January 4. Received 1994 December 29; in original form 1994 October 26

## ABSTRACT

The mass density field in the local universe, recovered by the POTENT method from peculiar velocities of  $\sim 3000$  galaxies, is compared with the density field of optically selected galaxies. Both density fields are smoothed with a Gaussian filter of radius  $12h^{-1}$  Mpc. Under the assumptions of gravitational instability and a linear biasing parameter  $b_O$  between optical galaxies and mass, we obtain  $\beta_O \equiv \Omega^{0.6}/b_O = 0.74 \pm 0.13$ . This result is obtained from a regression of POTENT mass density on optical density after correcting the mass density field for systematic biases in the velocity data and POTENT method. The error quoted is just the  $1\sigma$  formal error estimated from the observed scatter in the density–density scatterplot; it does not include the uncertainty due to cosmic scatter in the mean density or in the biasing relation. We do not attempt a formal analysis of the goodness of fit, but the scatter about the fit is consistent with our estimates of the uncertainties.

**Key words:** galaxies: distances and redshifts — galaxies: clustering — dark matter — large-scale structure of Universe

## 1 INTRODUCTION

With the advent of large-scale redshift and peculiar velocity surveys, it has become possible to investigate the relationship between the distribution of mass and galaxies on supercluster scales. Assuming that structures grow through gravitational instability (GI), then, on large scales where linear theory is applicable, the peculiar velocity of a galaxy is proportional to its peculiar gravitational acceleration. The constant of proportionality depends on the density parameter,  $\Omega$ , like  $f(\Omega) \simeq \Omega^{0.6}$  (e.g. Peebles 1980). The acceleration scales with the amplitude of the mass density fluctuation field, so, if we assume that the density contrast of optically selected galaxies,  $\delta_O$ , is related to the density contrast of mass,  $\delta$ , by linear biasing  $\delta_O = b_O \delta$ , then the appropriate scaling factor between peculiar velocity and galaxy density becomes  $\beta_O \equiv f(\Omega)/b_O$ . The determination of  $\beta_O$  is the goal of this paper.

There are two general ways to obtain  $\beta_O$  from peculiar velocity data and the density field as derived from a galaxy redshift survey. Each method has advantages and disadvantages. One approach is to predict radial peculiar velocities from the density field via gravity and adjust  $\beta_O$  for the best fit to the peculiar velocity data (e.g. Huchra 1988 and references therein; Strauss 1989; Kaiser et al. 1991;

Shaya, Tully & Pierce 1992; Hudson 1994b; Willick et al., in preparation). A potential error in such velocity–velocity comparisons arises from the non-locality of the predicted velocities, which are affected by the density field in unsurveyed regions such as the Galactic Zone of Avoidance and distant regions. Another potential source of error is the fact that the computation of the predicted velocities involves smoothing, while they are compared to raw, unsmoothed peculiar velocity data.

An alternative approach is to compare density fields smoothed in a similar way. In linear theory, the mass density fluctuation can be determined from the divergence of the peculiar velocity field,  $\mathbf{v}$ ,

$$\delta = -f^{-1} \nabla \cdot \mathbf{v}, \quad (1)$$

and a generalized approximation is valid in the quasi-linear regime (see Section 2 below). The comparison of densities in the linear regime yields  $\beta_O$ , and in the quasi-linear regime it allows a determination of  $b_O$  for a given value of  $\Omega$ . The main advantages of this approach are the locality of the comparison (on scales larger than the smoothing scale), and the fact that similar smoothing is applied to *both* fields at a scale on which linear or quasi-linear theory is applicable. This approach was taken by Dekel et al. (1993, hereafter DBY93), who compared the mass density derived by POTENT (Dekel,

Bertschinger & Faber 1990, hereafter DBF; Bertschinger et al. 1990) from the peculiar velocity sample of Burstein (1990, Mark II) to the density field of galaxies drawn from the *IRAS* 1.9-Jy redshift survey (Strauss et al. 1990, 1992). Dekel et al. used an elaborate likelihood analysis to find that the data were consistent with the assumptions of GI and linear biasing, and estimated  $\beta_I = 1.3 \pm 0.3$ .

The goal of this paper is to estimate  $\beta_O$ , under the assumption of GI and linear biasing, by a straightforward comparison of the density field of *optically selected* galaxies and the mass density field as determined by an improved POTENT procedure applied to an extended and newly calibrated data set.

The outline of this paper is as follows. The mass density field is first determined by applying POTENT to a data set of peculiar velocities containing  $\sim 3000$  galaxies. The velocity data, some details of the POTENT method, and in particular the biases introduced in using sparse, non-uniform and noisy radial peculiar velocities to obtain a mass density field are summarized in Section 2. The optical density field is then described in Section 3. In Section 4, we estimate  $\beta_O$  by means of a linear regression of the POTENT density fluctuation,  $\delta_P$ , on the optical density fluctuation,  $\delta_O$ , eliminating biases in the POTENT procedure, and evaluate the robustness of the result. We also demonstrate the difficulty of separating  $\Omega$  and  $b_O$  via non-linear effects. Finally, in Section 5, we summarize our results and discuss them in light of other determinations.

## 2 POTENT DENSITY FIELD

The sample of galaxies with measured redshifts and forward Tully-Fisher or  $D_n - \sigma$  (hereafter collectively TF) inferred distances used in this paper is a preliminary version of the Mark III catalogue. The calibration and compilation of the several data sets comprising the Mark III catalogue are described in detail by Willick et al. (1995 and in preparation). The elliptical data (Lucrey & Carter 1988; Faber et al. 1989; Dressler, Faber & Burstein 1991) are the same data previously compiled by Burstein (1990) for the Mark II catalogue. The spiral data contain the nearby Mark II data of Aaronson et al. (1982) as revised by Tormen & Burstein (1995), and newer extended data from Han (1991), Han & Mould (1992), Mould et al. (1991, 1993), Willick (1991), Courteau (1992), and Mathewson, Ford & Buchorn (1992). The sample consists of about 3000 galaxies grouped into  $\sim 1150$  objects.

Inhomogeneous Malmquist (IM) bias affects the determination of  $\Omega$  (or  $\beta$ ) from TF data when the analysis, as in POTENT, combines neighbouring galaxies in inferred-distance space (e.g. Willick 1991, 1994; Hudson 1994a; Dekel 1994). The distance errors, combined with galaxy-density variations along the line of sight, systematically enhance the inferred velocity gradients and thus the inferred density fluctuations and  $\Omega$  or  $\beta$ . The IM bias is first reduced and then corrected by a new procedure that has been tested using mock peculiar velocity catalogues drawn from N-body simulations. The mock catalogues are constructed in a way which mimics the non-uniform sampling and the noise of the real data. The IM bias correction procedure is discussed in detail by Dekel et al. (in preparation, hereafter D95c) and is only summarized briefly here. First, the galaxies are

grouped heavily in redshift space, while correcting for ‘selection’ bias (Willick 1991, 1994). This grouping reduces the distance error of each group of  $N$  members to  $\Delta/\sqrt{N}$ , where  $\Delta \approx 0.15 - 0.21$  and  $0.21$  for spirals and ellipticals respectively. The IM bias scales like the square of the distance error, so this grouping significantly reduces the IM bias. Then, the noisy inferred distance of each object,  $d$ , is replaced by the expectation value of the true distance  $r$  given  $d$  (e.g. Willick 1991, equation 5.70):

$$E(r|d) = \frac{\int_0^\infty r^3 n(r) \exp\left(-\frac{[\ln(r/d)]^2}{2\Delta^2}\right) dr}{\int_0^\infty r^2 n(r) \exp\left(-\frac{[\ln(r/d)]^2}{2\Delta^2}\right) dr}. \quad (2)$$

For single, ungrouped galaxies,  $n(r)$  should be the number density of galaxies in the underlying distribution from which galaxies were selected for the sample (assuming they were selected by quantities that do not explicitly depend on  $r$ ). In cases where the sample is redshift-limited,  $n(r)$  is truncated at the appropriate distance. In a grouped sample, the density run  $n(r)$  is multiplied by appropriate grouping/selection correction factors for the grouped and ungrouped objects respectively. (see D95c for details). This procedure is found to reduce the IM bias in the mock catalogues to the level of a few per cent. As an approximation to  $n(r)$  we use for spirals the density of *IRAS* 1.2-Jy galaxies (Fisher 1992), and for ellipticals the density of early-type galaxies derived by Hudson (1993a, see also Section 3 below), both smoothed with a Gaussian filter of radius  $500 \text{ km s}^{-1}$ . The final IM correction typically amounts to less than 10 per cent in the  $1200 \text{ km s}^{-1}$  smoothed density field described next.

The POTENT procedure takes these discrete and noisy radial velocity data,  $u_i$  at positions  $\mathbf{x}_i$ , and first smoothes them with a Gaussian window of radius  $1200 \text{ km s}^{-1}$  (DBF; Dekel et al., in preparation, hereafter D95a, D95b). It then applies the gravitational ansatz of potential flow to recover the missing transverse components of the velocity field (Bertschinger & Dekel 1989). Finally, it applies a quasi-linear approximation with an assumed value of  $\Omega$  to reconstruct the associated field of mass-density fluctuations. The quasi-linear generalization of the linear approximation to gravitational instability is the solution of the continuity equation under the Zel’dovich approximation in Eulerian space (Nusser et al. 1991),

$$\delta_c(\mathbf{x}) = \|\mathbf{I} - f^{-1} \partial \mathbf{v} / \partial \mathbf{x}\| - 1, \quad (3)$$

where the bars denote the Jacobian determinant, and  $\mathbf{I}$  is the unit matrix.

The non-trivial step in POTENT is the *smoothing* of the data into a radial velocity field  $u(\mathbf{x})$ . This smoothing procedure is described and tested in detail elsewhere (DBF; D95b; Kolatt et al., in preparation). The procedure is only briefly summarized here with emphasis on the new features of the method. The aim is to reproduce the  $u(\mathbf{x})$  that would have been obtained had the true three-dimensional velocity field  $\mathbf{v}(\mathbf{x})$  been sampled densely and uniformly and smoothed with a spherical Gaussian window of radius  $R_s$ . With the discrete data available,  $u(\mathbf{x}_c)$  is taken to be the value at  $\mathbf{x} = \mathbf{x}_c$  of an appropriate parametric local velocity model  $\mathbf{v}(\alpha_k, \mathbf{x} - \mathbf{x}_c)$  obtained by minimizing the weighted sum of residuals

$$\sum_i W_i [u_i - \hat{\mathbf{x}}_i \cdot \mathbf{v}(\alpha_k, \mathbf{x}_i - \mathbf{x}_c)]^2, \quad (4)$$

in terms of the parameters  $\alpha_k$  within an appropriate local window  $W_i = W(\mathbf{x}_i, \mathbf{x}_c)$ . The local velocity model and the weighting needed in order to minimize random errors and systematic biases are chosen as follows.

Even for the case of dense, uniform sampling the recovered  $u(\mathbf{x})$  field will in general suffer from ‘window bias’. Unless  $R_s$  is much smaller than the distance from the origin to the centre of the window,  $r_c$ , the radial peculiar velocity data,  $u_i$ , cannot be averaged as scalars because the directions  $\hat{\mathbf{x}}_i$  differ from  $\hat{\mathbf{x}}_c$ , so  $u(\mathbf{x}_c)$  requires a fit of a local 3D velocity model. The original POTENT method (DBF) used the simplest local model,  $\mathbf{v}(\mathbf{x}) = \mathbf{B}$ , where  $\mathbf{B}$  is a uniform velocity, for which the solution can be expressed explicitly in terms of a tensor window function. The tensorial correction to the spherical window has conical symmetry, weighting more heavily objects of large  $\hat{\mathbf{x}}_i \cdot \hat{\mathbf{x}}_c$ . This window deformation introduces a bias which is particularly severe nearby, where  $R_s/r_c$  is not small, and in places where the velocity has a large divergence or convergence transverse to the line of sight. For example, a converging flow in a plane transverse to the line of sight would be biased to show an artificial component towards the origin. For the current peculiar velocity data, the resulting bias in the smoothed radial peculiar velocity field reaches a maximum value of  $\sim 300 \text{ km s}^{-1}$  at the position of the Great Attractor. A way to reduce this bias is by generalizing  $\mathbf{v}(\mathbf{x})$  into a *linear* velocity model,  $\mathbf{v}(\mathbf{x}) = \mathbf{B} + \mathbf{L} \cdot (\mathbf{x} - \mathbf{x}_c)$ , with  $\mathbf{L}$  a symmetric tensor, which ensures local irrotationality. The linear terms tend to ‘absorb’ most of the bias, leaving  $\mathbf{v}(\mathbf{x}_c) = \mathbf{B}$  less biased. Unfortunately, a high-order model tends to pick undesired small-scale noise, especially where the data are sparse and noisy. The optimal compromise is found to be a first-order model fit out to  $r = 40h^{-1} \text{ Mpc}$ , smoothly changing to a zeroth-order fit beyond  $60h^{-1} \text{ Mpc}$  (D95b).

Unfortunately, the real peculiar velocity data are both non-uniformly sampled and noisy. If the true velocity field is varying within the effective window, then non-uniform sampling will introduce a sampling-gradient (SG) bias. This bias occurs because the smoothing is weighted by the distribution of sampled galaxies whereas the aim is equal-volume weighting. One should weight each object by the local volume it ‘occupies’,  $V_i$ . We adopt  $V_i \propto R_4^3$  where  $R_4$  is the distance to the fourth neighbouring object. This weighting procedure (termed P0) is found from simulations to reduce the SG bias in the Mark III sample to negligible levels out to a typical depth of  $60h^{-1} \text{ Mpc}$  (away from the Galactic Zone of Avoidance). The  $R_4(\mathbf{x})$  field will serve later as a flag for poorly sampled regions, to be excluded from any quantitative analysis.

The ideal weighting for reducing the effect of Gaussian noise in the peculiar velocity measurements,  $\sigma_i$ , requires weights  $W_i \propto \sigma_i^{-2}$ , but this spoils the volume weighting and biases  $u$  towards its values at smaller  $r_i$  and at nearby clusters where the errors are small. A successful compromise (termed P1) is to weight by both, i.e.

$$W(\mathbf{x}_i, \mathbf{x}_c) \propto V_i \sigma_i^{-2} \exp[-(\mathbf{x}_i - \mathbf{x}_c)^2 / 2R_s^2]. \quad (5)$$

The difference between the recovered fields using the P0 and P1 weighting schemes can serve as an indicator for the

magnitude of the systematic uncertainty still remaining in the POTENT recovery.

The errors in the recovered fields, due to scatter in the distance indicator and measurement errors, are assessed by Monte Carlo simulations, where the input distances are perturbed at random using a Gaussian of standard deviation  $\sigma_i$  [in fact  $(\sigma_i^2 + \sigma_f^2)^{1/2}$ , where  $\sigma_f \sim 200 \text{ km s}^{-1}$  is the local dispersion of velocities in the ‘field’] before being fed into POTENT. The error in  $\delta_P$  at a grid point is estimated by the standard deviation of the recovered  $\delta_P$  over the Monte Carlo simulations,  $\sigma_\delta$ . In the well-sampled regions, which extend in Mark III out to  $40\text{--}60h^{-1} \text{ Mpc}$ , the errors are  $\sigma_\delta \approx 0.1\text{--}0.3$ , but they may blow up in certain regions at large distances. To exclude noisy regions, any quantitative analysis should be limited to points where  $\sigma_\delta$  is within certain limits (see Section 4.1 below).

There exists a fundamental freedom in determining the *zero-point* TF parameter which fixes the distance scale in units of  $\text{km s}^{-1}$ . A change of this zero-point multiplies all distances by a factor  $(1+\epsilon)$  while the redshifts are fixed. This is equivalent to adding a monopole Hubble-like component  $-\epsilon r$  to the peculiar velocities  $\mathbf{v}$ , and an offset  $3\epsilon f^{-1}(\Omega)$  to  $\delta$  ( $\approx -f^{-1} \nabla \cdot \mathbf{v}$ ). The zero-point Hubble flow has tentatively been determined in the Mark III data from the 38 spiral clusters, which are distributed across the the sample volume. After processing through POTENT, the zero-point is fine-tuned by minimizing the volume-weighted variance of the recovered peculiar velocity field (equivalent in the linear regime to enforcing  $\langle \delta \rangle = 0$ ) in a ‘fair’ volume, taken here to be a sphere of radius  $6000 \text{ km s}^{-1}$ . In fact, the zero-point adopted has no effect on the determination of  $\beta$  below (Section 4.2).

The POTENT density field (D95a) is shown in the left-hand panels of Figs 1 and 2. Fig. 1 shows contour plots of the smoothed density field in slices parallel to the Supergalactic Plane. Fig. 2 shows the density field in the Supergalactic Plane as a surface plot where the height of the surface above the plane of the plot is proportional to density.

### 3 THE OPTICAL DENSITY FIELD

We now summarize the optical galaxy sample, completeness corrections and the method used to reconstruct the density field of optical galaxies (for further details see Hudson 1993a). The basic catalogue of 12 439 galaxies covering 67 per cent of the sky is a merger of the diameter-limited UGC (Uppsala General Catalogue of Galaxies: Nilson 1973) and ESO (The ESO-Uppsala Survey of the ESO(B) Atlas: Lauberts 1982) catalogues. The UGC catalogue is corrected for incompleteness for diameters between 1.2 and 1.6 arcmin, and the ESO catalogue is complete at diameters larger than 1.4 arcmin (Hudson & Lynden-Bell 1991). The 6747 redshifts in the sample were obtained from the major redshift surveys, i.e., CfA1 (Davis & Huchra 1982; Huchra et al. 1983), SSRS (da Costa et al. 1988, 1991), SPS (Dressler 1991), and Perseus–Pisces (Giovanelli & Haynes 1985; Giovanelli et al. 1986), and from the redshift compilations of Huchra (1990) and Fairall & Jones (1991). The variable completeness of the redshift sample is mapped as a function of angular diameter and position on the sky. These completeness functions are used in conjunction with the UGC and ESO diameter func-

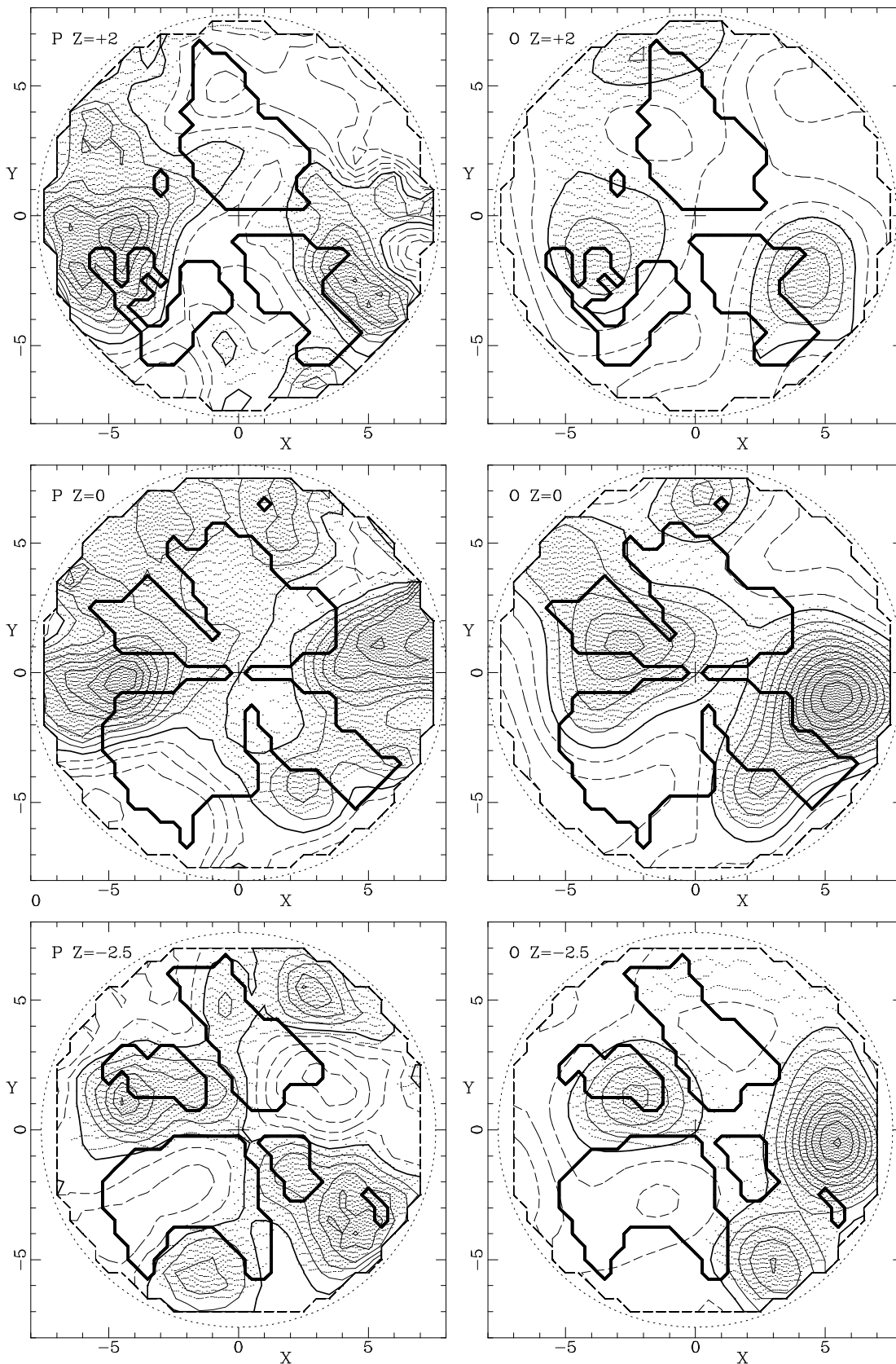


**Figure 1.** The density fields in slices parallel to the Supergalactic Plane. The left-hand panels show the POTENT mass density field and the right-hand panels show the density field of optical galaxies, both smoothed with a Gaussian filter of radius  $1200 \text{ km s}^{-1}$ . The contour levels are in steps of  $\Delta\delta = 0.2$ . The medium-thickness contours indicate the mean density, thin solid contours show overdense regions and dashed contours show underdense regions. The heavy contours indicate the boundary of the ‘Large’ comparison volume (see Section 4.1 for details). The dotted circle has a radius of  $8000 \text{ km s}^{-1}$ . The top row shows the slice at Supergalactic  $Z = 2000 \text{ km s}^{-1}$ .

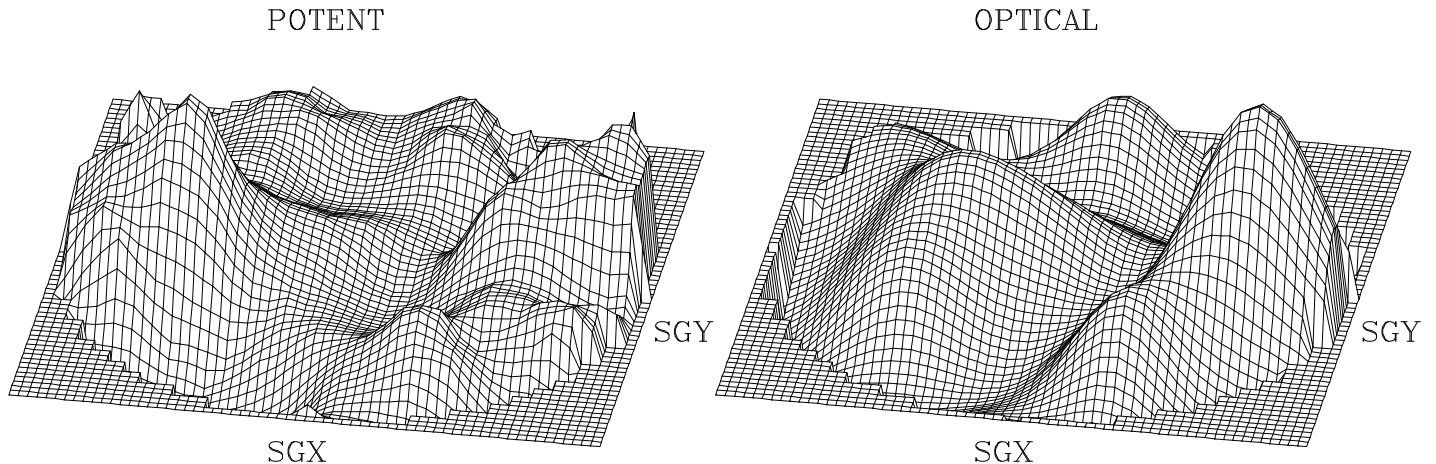


**Figure 2.** Surface plots of the density fields in the Supergalactic Plane. The left-hand panel shows the POTENT mass density field and the right-hand panel shows the density field of optical galaxies, both smoothed with a Gaussian filter of radius  $1200 \text{ km s}^{-1}$ . The density contrast is proportional to the height of the surface above (or below) the plane of the plot.

tions (Hudson & Lynden-Bell 1991) to assign a weight to each galaxy in the redshift sample to compensate for those galaxies in the underlying density field that were not selected.

We then iteratively transform from redshift space to distance space by self-consistently calculating linear peculiar velocities from the optical density field (cf. Yahil et al. 1991). The value of  $\beta_{\text{O}}$  is fixed at 0.5 for these iterations, but the resulting optical density field does not depend sensitively on this choice. Indeed, had we used  $\beta_{\text{O}} = 0.75$  in the iteration, our final result for  $\beta_{\text{O}}$  would have increased by only 0.03.

There are no data in the Zone of Avoidance  $|b| < 12^\circ$  and the ‘missing’ equatorial strip between the UGC and ESO catalogues ( $-17.5^\circ < \text{Dec.} < -2.5^\circ$ ). We adopt a simple scheme for filling in this ‘masked’ area: the ‘cloned mask’ model (cf. Lynden-Bell, Lahav & Burstein 1989) attempts a crude interpolation in the galactic and equatorial missing strips by copying the set of weighted galaxies in adjacent strips and shifting these ‘clones’ in galactic latitude and declination respectively.

In the final step, the weighted set of points is smoothed to yield an optical density field. We use the same smoothing filter as used for the POTENT density field, namely a Gaussian filter with a  $1200 \text{ km s}^{-1}$  radius, and we sample the density fields on the same  $500 \text{ km s}^{-1}$  grid. In the final comparison, we exclude all grid points within the masked area (see Section 4.1 below). However, note that, due to the smoothing, the density assumed within the masked region will affect the density at adjacent grid points. Therefore, the ‘cloning’ procedure is preferred over less realistic schemes such as the ‘average mask model’ in which the masked region is set to the average density.

The mean density of optical galaxies is needed in order to calculate the density contrast,  $\delta_{\text{O}} = (\rho_{\text{O}} - \bar{\rho}_{\text{O}})/\bar{\rho}_{\text{O}}$ . In this paper, we estimate the mean optical density by averaging over optical galaxies in the unmasked volume within  $6000 \text{ km s}^{-1}$ . This volume is close to the typical depth of the final comparison volume (see Section 4.1 below).

The optical density field is shown in the right-hand panels of Figs 1 and 2.

## 4 DETERMINATION OF $\beta_{\text{O}}$

In the determination of the parameter  $\beta_{\text{O}}$ , our philosophy is to carry out as simple an analysis as possible. We use simplifying approximations where we believe, based on our experience with mock data sets, that any biases introduced by these approximations are small compared to the unavoidable uncertainties due to the random errors, the limited volume sampled (cosmic scatter), the unknown complexity of the true biasing relation, and the remaining uncorrected effects of non-linear gravity. We deviate from a straightforward analysis only when faced with a significant bias. The approximations made in this analysis are tested using mock catalogues elsewhere (Dekel et al., in preparation, hereafter D95d).

In Section 4.1, we define the volume used for the comparison. In Section 4.2, we discuss the method of fit, based on a simple  $\chi^2$  statistic, and the effective number of independent volumes within the comparison volume. In Section 4.3, we discuss the issue of SG bias and how it biases the determination of  $\beta_{\text{O}}$ , and in Section 4.4 we discuss the scatter in the density–density plots. In Section 4.5, we present results for  $\beta_{\text{O}}$  assuming  $\Omega = 1$ , and in Section 4.6 we discuss the results for  $\Omega = 0.3$ .

### 4.1 Definition of the comparison volume

The density–density comparison in this paper is local (unlike the velocity–velocity comparison) and the POTENT data are weighted inversely by their local errors. Consequently, we are free to choose the volume considered in the density–density comparison. In selecting the volume, we aim to minimize the SG bias and the random errors, and to maximize the number of effectively independent volumes used in the comparison. In practice, there is an obvious trade-off between these two goals. We therefore limit the volumes by  $R_4$ , in order to minimize the SG bias, and by  $\sigma_\delta$ , in order to eliminate regions with very large random errors. Furthermore, we use only the grid points that are within  $7000 \text{ km s}^{-1}$  and outside the masked region of the optical density field. In order

**Table 1.** Comparison volumes.

Sample	$R_4$ km s <sup>-1</sup>	$\sigma_\delta$	$N_{\text{grid}}$	$N_{\text{eff}}$
P1 S	< 1200	< 0.25	2197	22.1
P1 L	< 1500	< 0.30	3334	31.2
P0 S	< 1200	< 0.30	1712	18.0
P0 L	< 1500	< 0.40	2934	28.9

to investigate how our results depend on specific choices for these parameters, we consider two comparison volumes for each of the POTENT methods (P0 and P1). We refer to these as the S (‘small’) and L (‘large’) volumes. Table 1 lists the  $R_4$  and  $\sigma_\delta$  limits, the number of grid points (from a cubic grid of 500 km s<sup>-1</sup> spacing) used in the comparison, and the effective number of independent points in the fit (discussed below) for the four volumes considered.

The limits of the P1L volume are indicated in Fig. 1. The radial indentations in the comparison volume arise from the optical mask (i.e. the Zone of Avoidance and the ‘missing’ equatorial strip). The irregular outer limit is determined by the inhomogeneity in the POTENT data. The P1S volume covers approximately 67 per cent of the sky and has a total volume of (6500 km s<sup>-1</sup>)<sup>3</sup>. Its outer boundary (outside of the Zone of Avoidance) lies between 3000 and 7000 km s<sup>-1</sup>, depending on direction.

## 4.2 Method of fit

A visual comparison between the left- and right-hand panels of Fig. 1 and Fig. 2 shows a reasonable resemblance between the large-scale features of the POTENT and optical density fields. Displacements of density peaks are seen at a similar level in the mock catalogues as a result of the sparse, non-uniform and noisy sampling. Assuming GI and no systematic errors, the mass density – optical density diagram is a direct representation of the biasing relation (for the value of  $\Omega$  used in the POTENT reconstruction). Assuming a linear biasing relation with no scatter, we expect the densities to be related by

$$\delta_{\text{P}} = \lambda \delta_{\text{O}} + c \quad (6)$$

where the slope,  $\lambda$ , is just equal to  $b_{\text{O}}^{-1}$ . The zero-point,  $c$ , allows for a relative offset in the mean density of the two density fields. This parameter is necessary because the volumes within which we have separately normalized the POTENT and optical density fields are slightly different from each other.

The random errors in the inferred peculiar velocities introduce an error in the POTENT density,  $\sigma_\delta$ , so of course we expect some scatter in the POTENT – optical density diagram. We have estimated the random shot-noise errors in the optical density field using the technique of bootstrap resampling. We find these errors to be typically  $\sim 0.07$ , and always less than half the random errors of the POTENT density field at a given grid point. In the following analysis we assume that all errors are in the POTENT density field, and thus regress  $\delta_{\text{P}}$  on  $\delta_{\text{O}}$  in the determination of  $\lambda$ .

If the grid points were independent of each other and if POTENT errors were Gaussian, we could construct a reduced  $\chi^2$  statistic,

$$S = N_{\text{grid}}^{-1} \sum_i^{N_{\text{grid}}} \frac{(\delta_{\text{P}} - \lambda \delta_{\text{O}} - c)^2}{\sigma_{\text{P}}^2}, \quad (7)$$

where the sum is over all  $N_{\text{grid}}$  grid points in the comparison volume and  $\sigma_{\text{P}}$  is the error in the POTENT density.

In practice, we sample the density fields on a grid with a much finer spacing (500 km s<sup>-1</sup>) than the smoothing radius (1200 km s<sup>-1</sup>), so the grid points are not independent. The effective number of independent volumes in the  $\chi^2$  fit can be estimated by

$$N_{\text{eff}}^{-1} = N_{\text{grid}}^{-2} \sum_j^{N_{\text{grid}}} \sum_i^{N_{\text{grid}}} \exp(-r_{ij}^2/2R_s^2) \quad (8)$$

(DBY93). The values of  $N_{\text{eff}}$  for each comparison volume are given in Table 1. We find that with our grid spacing and smoothing we have oversampled the volume by a factor  $F = N_{\text{grid}}/N_{\text{eff}} \sim 100$ . Thus our data points would be independent if sampled on a grid with spacing  $F^{1/3} \times 500 \text{ km s}^{-1} = 2320 \text{ km s}^{-1}$ , which is about twice the smoothing length. Due to the oversampling, the appropriate statistic to use is a corrected  $\chi_{\text{eff}}^2 \equiv N_{\text{eff}} S$ , which is distributed like  $\chi^2$  with  $N_{\text{d.o.f}} = N_{\text{eff}} - 2$  degrees of freedom. This statistic is used to assess the errors on  $\lambda$  and  $c$ , as a simple approximation to the elaborate and more accurate likelihood analysis using Monte Carlo simulations (e.g. DBY93).

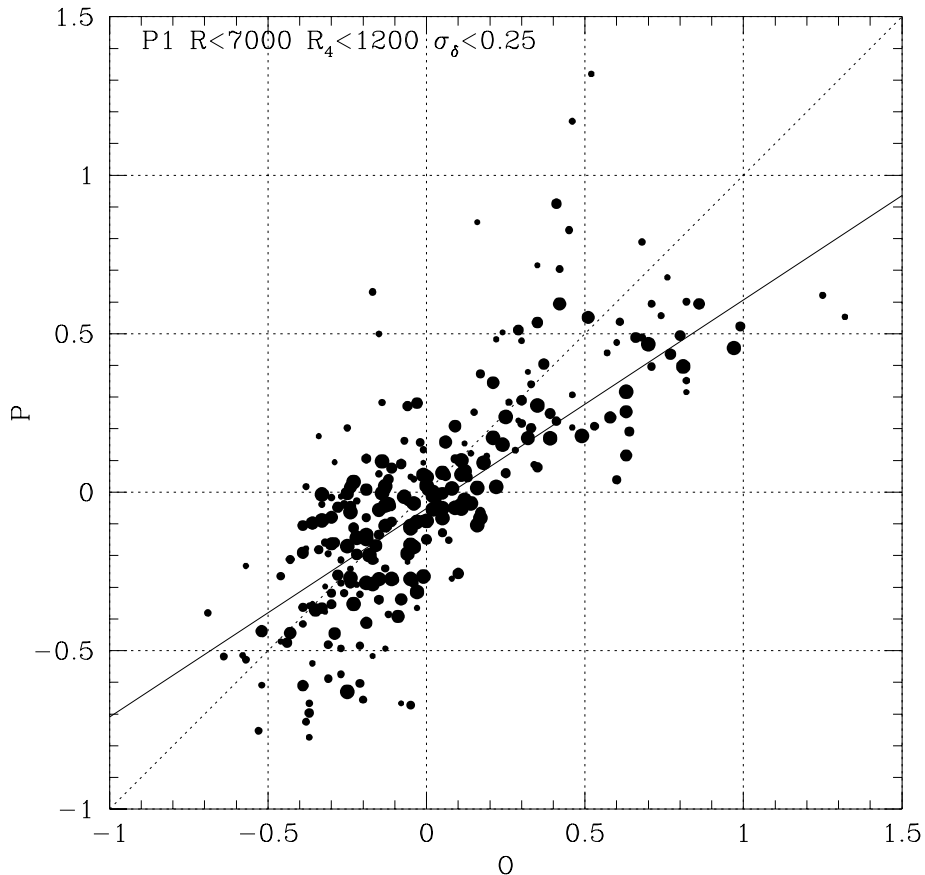
## 4.3 Correction of biases in POTENT

Fig. 3 shows the comparison between  $\delta_{\text{P}}$  (P1S) and  $\delta_{\text{O}}$ . If we set  $\sigma_{\text{P}} = \sigma_\delta$  (the random error in the POTENT density) in equation (7), we obtain the result  $\lambda = 0.66 \pm 0.08$ ,  $c = -0.05 \pm 0.02$ . The quoted errors are the formal errors from the  $\chi^2$  fit. This fit is shown as the solid line in Fig. 3.

However, it would be premature to adopt these results as our best estimate of  $\beta_{\text{O}}$  because this estimate is known to be biased. DBY93 tested the POTENT method by comparing the smoothed *IRAS* density field to the density field recovered by the POTENT method from the unsmoothed *IRAS*-predicted peculiar velocities with  $\Omega = 1$  and  $b_{\text{I}} = 1$ . The *IRAS* velocity and density fields served there as a model for a general gravitating system. DBY93 found that, in the limit of dense, uniform sampling, they recovered a slope close to the true slope of unity with very small scatter (see e.g. their fig. 4c). However, when they sampled the *IRAS* peculiar velocity field at only the positions of the galaxies in the Mark II peculiar velocity data sample, they found an increased scatter and a biased slope of 0.66. Thus, the systematic errors in the POTENT procedure are correlated with the density field and introduce a bias in the slope, tending to reduce it.

Following DBY93, we use as a test case the optical density field itself from which we calculate predicted peculiar velocities via gravity at the estimated distance of each galaxy in the peculiar velocity data set. Specifically, we begin by smoothing the optical density field with a Gaussian filter of 500 km s<sup>-1</sup> radius. Peculiar velocities are calculated using the prescription of Nusser et al. (1991), i.e.

$$\mathbf{v}(\mathbf{r}) = \frac{f(\Omega)}{4\pi b_{\text{O}}} \int \frac{\delta_{\text{O}}(\mathbf{r}')}{1 + 0.18b_{\text{O}}^{-1}\delta_{\text{O}}(\mathbf{r}')} \frac{\mathbf{r}' - \mathbf{r}}{|\mathbf{r}' - \mathbf{r}|^3} d^3\mathbf{r}', \quad (9)$$



**Figure 3.** The density–density scatterplot with the optical density (O) on the horizontal axis and the POTENT mass density (P) on the vertical axis. The densities are sampled on a  $1000 \text{ km s}^{-1}$  grid within the ‘P1 Small’ volume, thus the plotted points oversample the number of independent volumes by a factor  $\sim 12$ . The areas of the plotted points have been scaled with the inverse squares of their errors. The solid line is the result of the weighted linear regression of  $\delta_P$  on  $\delta_O$ ; a dotted line of slope unity is also shown for reference.

at the observed positions of the galaxies in the Mark III data set. For the  $\Omega = 1$  case, we adopt a biasing parameter of  $b_O = 1.3$ , which ends up consistent with our final result. These predicted peculiar velocities are then used as the input to the POTENT procedure with  $1090 \text{ km s}^{-1}$  Gaussian smoothing which, when added in quadrature with the  $500 \text{ km s}^{-1}$  smoothing radius of the input field, ensures a total Gaussian smoothing of  $1200 \text{ km s}^{-1}$ . The resulting mass density fluctuation field is then multiplied by  $b_O$  to obtain the corresponding field of optical galaxies. The result of this procedure, which we label  $P(O)$ , is a galaxy density field which is affected by SG bias in the same way as the POTENT mass density field recovered from the Mark III data. Fig. 4 compares the density fields of POTENT [P], optical through POTENT [P(O)], and raw optical [O].

In Fig. 5, we show the  $P(O) - O$  scatterplot for this test case. If the same weights at each grid point as used in the  $P - O$  comparison above are adopted, the slope of best fit is 0.88. This bias in the slope is smaller than that found by DBY93 due to the increase in sampling density of the peculiar velocity data, the improvements in the POTENT

procedure, and the more accurate adjustment of the POTENT smoothing scale to a total of  $1200 \text{ km s}^{-1}$ .

#### 4.4 Scatter in the POTENT – optical density diagram

Before turning to the results of the fits, we must first discuss the scatter in the density–density diagram, in order to verify that the assumed model of GI plus linear biasing is indeed consistent with the data. We find that, by setting  $\sigma_P$  equal to the error in the Monte Carlo simulations  $\sigma_\delta$ , we obtain  $\chi_{\text{eff}}^2 \gtrsim 2N_{\text{eff}}$ , which is apparently too large for an acceptable fit. This could be a result of underestimating the errors. Indeed, it is likely that there are other sources of error, predominantly in the POTENT density field, which are not accounted for by the Monte Carlo perturbations of the distances. We therefore allow for additional errors via an additional parameter,  $\sigma_{\text{add}}$ . The additional errors may or may not be correlated with  $\sigma_\delta$ , so we assume a weak correlation by adding *linearly*:  $\sigma_P = \sigma_{\text{add}} + \sigma_\delta$ . We then adjust  $\sigma_{\text{add}}$  so that  $\chi_{\text{eff}}^2 = N_{\text{eff}} - 2$ . The resulting values are  $\sigma_{\text{add}} = 0.06$  for the P1 comparisons, and  $\sigma_{\text{add}} = 0.04$  for the P0 compar-

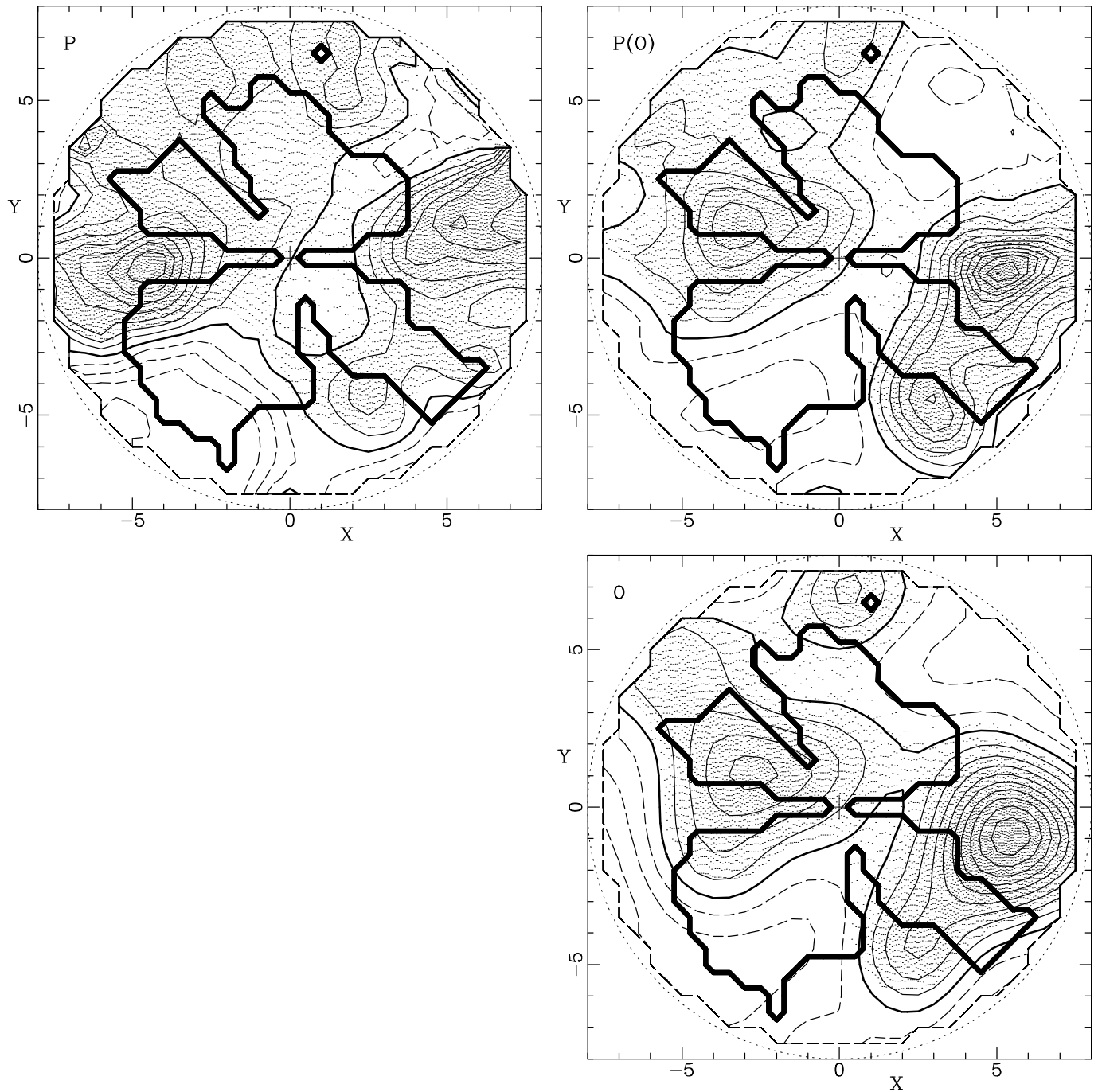


**Figure 4.** Maps of the density field in the Supergalactic Plane. The contour levels are as in Fig. 1. The upper left-hand panel shows the POTENT mass density field (P). The upper right-hand panel shows P(O), the POTENT recovery using predicted peculiar velocities from the optical density field at the positions of the Mark III data. The lower right-hand panel shows the optical density field (O). The difference between P(O) and O shows the effect of the biases discussed in the text.

isons. In Section 4.5, we show that the value of the slope,  $\lambda$ , is not significantly affected by our choice of  $\sigma_{\text{add}}$ . It is none the less necessary to include this additional error in order to obtain errors on the slope that are consistent with the observed scatter in the density–density plot.

Are these values of  $\sigma_{\text{add}}$  reasonable compared to the possible sources of scatter that are not included in  $\sigma_{\delta}$ , and

which are not eliminated by the comparison of P with P(O)? Additional sources of error might include the following.

- (i) The Monte Carlo estimates,  $\sigma_{\delta}$ , may underestimate the total errors in the POTENT density field. We have made a preliminary test of these errors using an ungrouped version of the mock catalogue described above. We have compared densities obtained from applying the POTENT procedure to

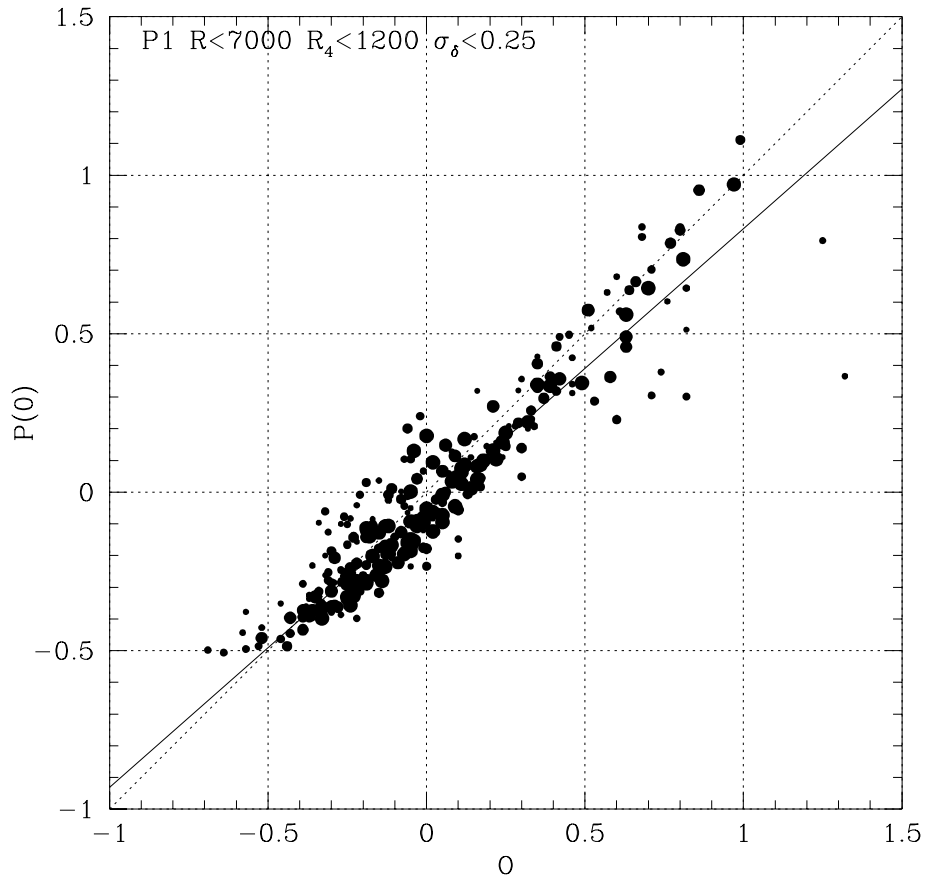


**Figure 5.** The density–density scatterplot with optical density ( $O$ ) plotted on the horizontal axis and  $P(O)$ , the POTENT recovery using predicted peculiar velocities from the optical density field at the positions of the Mark III data, plotted on the vertical axis. The comparison volume, sampling and symbols are as in Fig. 3. The solid line is the weighted linear regression of  $\delta_{P(O)}$  on  $\delta_O$ ; a dotted line of slope unity is also shown for reference. The deviation from a slope of unity is due to the biases discussed in the text.

the unperturbed velocities of galaxies at their true distances and to the perturbed velocities at the perturbed positions, after correcting for IM bias. We find that in addition to the Monte Carlo errors,  $\sigma_\delta$ , we require  $\sigma_{\text{add}} = 0.03$  in order to obtain an acceptable value of  $\chi^2$ .

(ii) There may be errors in the POTENT density field due to imperfections in the inhomogeneous Malmquist bias corrections. An upper limit to these errors is estimated by the rms difference between the POTENT density fields corrected and uncorrected for IM, which is  $\sim 0.11$ .

(iii) There may be systematic errors in the optical density field due to interpolation (‘cloning’) into the unsampled regions. An upper limit to these errors is estimated by comparing the cloned mask density field to the average mask density field. Within the P1S comparison volume, the rms scatter between the cloned and average mask density fields is  $\sim 0.06$ . Spurious large-scale gradients may also exist at some level due to possible errors in matching the UGC and ESO data in the northern and southern hemispheres (see Hudson 1993b,1994b). We note, however, that the results for  $\beta_O$  from these two hemispheres separately are in perfect agreement with each other (see Section 4.5 below).

**Table 2.** Results of  $P - P(O)$  fits.

Sample	$\lambda$	$c$
<b>P1S</b>	<b><math>0.74 \pm 0.13</math></b>	<b><math>-0.01 \pm 0.04</math></b>
P1L	$0.78 \pm 0.13$	$-0.02 \pm 0.04$
P0S	$0.65 \pm 0.15$	$0.01 \pm 0.04$
P0L	$0.68 \pm 0.14$	$0.01 \pm 0.04$

(iv) The shot-noise error in the optical density, although smaller than the random errors in POTENT, is not negligible. Within  $6000 \text{ km s}^{-1}$ , the typical shot-noise error is  $\sim 0.07$ .

(v) Spatial variations in the efficiency of galaxy formation and deviations from a linear biasing relation would generate true, physical, scatter about an assumed linear biasing relation between galaxies and mass. A scatter of  $\sim 0.15$  in the optical galaxy density added in quadrature to the POTENT error would account for the additional scatter in Fig. 3.

Since these possible sources of scatter are of the same order as our adopted value of  $\sigma_{\text{add}}$ , we may conclude that there is no evidence for inconsistency between the data and the assumptions of GI and linear biasing, allowing us to proceed to the parameter fit.

#### 4.5 Results

The comparison between the POTENT density and the POTENT-recovered optical density  $P(O)$  removes the biases in the POTENT procedure and thus yields an unbiased estimate of  $\beta_O$ . As discussed above, we assume that the errors in the POTENT density field dominate. We therefore obtain the slope from a regression of  $\delta_P$  on  $\delta_{P(O)}$  with the POTENT error  $\sigma_P = \sigma_\delta + \sigma_{\text{add}}$ . The results of the fit for the PO and P1 (L and S) cases are summarized in Table 2. Fig. 6 shows the  $P - P(O)$  scatterplot for the P1S case. In all cases, the zero-point  $c$  is small and compatible with zero. We have made a number of tests to check the robustness of the value of  $\lambda$  derived from the regression of  $\delta_P$  on  $\delta_{P(O)}$ . The results of these tests are summarized below.

(i) The value of  $\lambda$  is insensitive to the details of the assumed POTENT errors, provided that the optical errors are negligible. For the P1S case, if we assume equal errors for all grid points, our resultant  $\lambda$  increases by only 3 per cent. Similarly, if we set  $\sigma_{\text{add}} = 0$ , then  $\lambda$  decreases by 5 per cent. If we fit by minimizing absolute deviation, which is less sensitive to outliers, then  $\lambda$  decreases by 3 per cent.

(ii) The value of  $\lambda$  is insensitive to the exact volume used, as indicated by the good agreement between the S and L volumes. A further check can be made by dividing the P1S volume into the northern celestial hemisphere (containing the Perseus–Pisces supercluster) and the southern hemisphere (containing the Great Attractor region). We find  $\lambda = 0.73 \pm 0.26$  and  $0.75 \pm 0.15$  for northern and southern hemispheres, respectively. In fact, this almost perfect agreement between these independent volumes may indicate that we have overestimated our random errors.

(iii) The results are insensitive to the details of the Malmquist corrections. As a test of these corrections, we have compared the optical density field to a POTENT density field in which the input data were corrected for Malmquist bias assuming a homogeneous galaxy density field (hereafter HM-corrected). Although in a few specific regions (e.g. Perseus–Pisces) the difference between the IM- and HM-corrected POTENT density fields is as large as  $\sim 30$  per cent in  $\delta_P$ , when averaged over all grid points in the comparison volume the net effect is small. We find that with the HM corrections  $\lambda$  is only 2 per cent higher than when IM corrections are used.

(iv) The values for  $\lambda$  are  $\sim 12$  per cent lower for the P0 case than for the P1 case. This is a crude measure of the typical systematic error associated with the POTENT procedure.

(v) We have compared the P1S case to a version of the optical density field in which the masked region was set to the average density before smoothing (the ‘average mask model’ from Hudson 1993a). The value of  $\lambda$  is  $\sim 15$  per cent higher than the result with the ‘cloned mask’ density field used here. Although the average mask model is unrealistic, it sets an upper limit on the systematic error arising from the treatment of the masked region.

Our estimate of  $\beta_O$ , adopting the P1S results of the  $\delta_P$  on  $\delta_{P(O)}$  regression, is  $\beta_O = 0.74 \pm 0.13$ , where the quoted  $1\sigma$  errors are the formal errors on the slope which are consistent with the scatter about the linear fit.

Note that if we assume that the ‘extra’ scatter in the density–density diagram lies in the optical density field, whether due to errors in the optical density field or due to a real physical effect, such as spatial variations in the efficiency of galaxy formation, then we must do a more elaborate regression which allows for errors in both the POTENT and optical density fields. As an example, if we set  $\sigma_{\text{add}} = 0$  and thus  $\sigma_P = \sigma_\delta$ , but allow for a 0.15 error in the optical density, the regression yields a slope  $\lambda = 1.00 \pm 0.17$  and an acceptable value of  $\chi_{\text{eff}}^2$ . In Section 5 we discuss the possibility that there may be significant scatter in the efficiency of galaxy formation.

#### 4.6 The dependence on $\Omega$

The POTENT reconstruction includes quasi-linear effects so, in principle, it should be possible to obtain some information on  $\Omega$ , independent of  $b_O$ . To test this idea, we have generated a POTENT reconstruction with  $\Omega$  set to the value 0.3. This is compared to a  $P(O)$  density field in which the predicted peculiar velocities are determined via equation (9) with  $\Omega = 0.3$ , and  $b_O = 0.7$  in the quasi-linear correction within the integral. The slope of the resulting fit is thus an estimate of  $b_O^{-1}$ .

We find a slope  $\lambda = b_O^{-1} = 1.63 \pm 0.33$ , corresponding to  $b_O = 0.61 \pm 0.12$  or  $\beta_O = 0.79 \pm 0.16$ . Thus, we recover essentially the same value of  $\beta_O$  as in the  $\Omega = 1$  case because we are only in the mildly non-linear regime. The scatter about the straight-line fit in the  $\Omega = 0.3$  case is marginally smaller than in the  $\Omega = 1$  case, but the improvement is not statistically significant. We conclude that, given the random and systematic errors, including the possible deviations from linear biasing, we cannot remove the degeneracy between  $\Omega$  and  $b_O$ . In order to rule out a low-density universe by these results, one has to appeal to external arguments such as the fact that the required degree of *anti-biasing* is physically implausible.

### 5 DISCUSSION AND SUMMARY

Our simple analysis does not allow a formal evaluation of goodness of fit between the data and the assumed model of GI and linear biasing, but we conclude, based on the expected random and systematic errors and the possible real scatter in the biasing relation, that the data and model are not in conflict. Note, however, that a non-gravitational origin to the peculiar velocities, which could invalidate the current analysis, cannot be ruled out. An apparent agreement between the POTENT density field and the galaxy density field can also occur in non-gravitational scenarios provided that the galaxy density field has developed from homogeneous initial conditions in a way that satisfies the continuity equation, and that the present-day velocity field is irrotational and proportional to the time-averaged velocity field (Babul et al. 1994).

Adopting the model of GI and linear biasing, our main goal has been to determine  $\beta_O$  on a scale of  $1200 \text{ km s}^{-1}$ . We find, from a regression of POTENT density on optical density, the result  $\beta_O = 0.74 \pm 0.13$  (formal  $1\sigma$  error). This result is robust to the details of the volume used, to the treatment of Malmquist bias, and to the actual value of  $\Omega$ . The regression

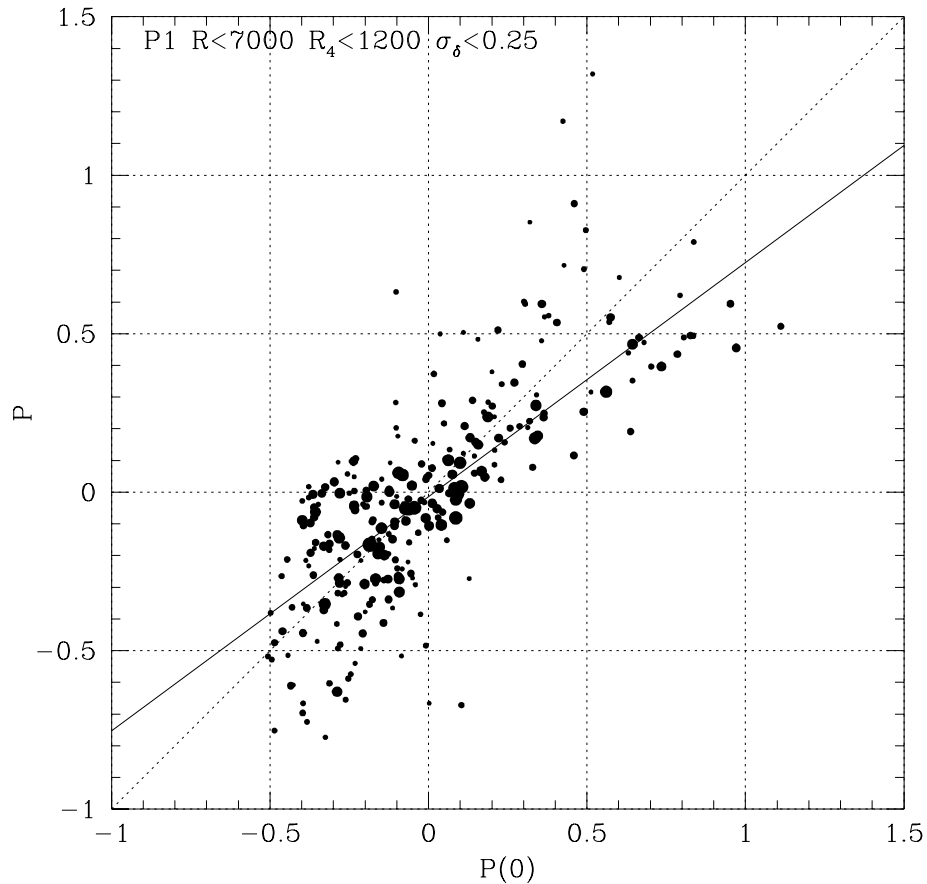


**Figure 6.** The density–density scatterplot with  $P(O)$  plotted on the horizontal axis and the POTENT density ( $P$ ) plotted on the vertical axis. The comparison volume, sampling and symbols are as in Fig. 3. The solid line is the straight line of best fit; a dotted line of slope unity is also shown for reference. The slope  $\lambda$  is our estimate of  $b_O^{-1}$  for  $\Omega = 1$ .

of POTENT density on optical density is insensitive to the relative weighting of grid points in the fit. The sensitivity of  $\beta_O$  to extreme changes in the POTENT weighting scheme is at the 12 per cent level. Its sensitivity to extreme changes in the way in which the optical density field is interpolated across of the Zone of Avoidance is at a similar level.

Non-linear effects on this scale are small compared to the uncertainties in the data, the analysis, and the biasing scheme, so we are unable to remove the degeneracy between  $\Omega$  and  $b_O$ . Our degenerate result corresponds to  $b_O = 1.35 \pm 0.23$  if  $\Omega = 1$ , and to  $\Omega = 0.61 \pm 0.18$  if  $b_O = 1$ . Low values of the density parameter ( $\Omega \lesssim 0.3$ ) would require optical galaxies to be significantly anti-biased with respect to mass.

One should be cautioned not to interpret the estimated value of  $\beta_O$  too literally. On top of the formal error of 0.13 and the systematic uncertainties of similar order, our estimate of  $\beta_O$  is subject to cosmic scatter in the mean density; the comparison volume of radius  $\lesssim 6000 \text{ km s}^{-1}$  may still be small for a ‘fair’ sample. This cosmic scatter arises because, in our analysis, both the peculiar velocity data input to POTENT *and* the mean density of optical galaxies are normalized within a volume of radius  $\sim 6000 \text{ km s}^{-1}$ . Note that while the free parameter  $c$  corrects for small differences in

the normalizing volumes of the POTENT and optical density fields, and consequent differences in the mean density of these fields with respect to each other, it does not necessarily correct to the universal density. Thus our result is a *local* value of  $\Omega$  measured within the comparison volume. The rms scatter of the mean density in such a volume is expected to be at the level of  $\sim 10 - 15$  per cent according to the fluctuation power spectra in conventional cosmological scenarios. Thus the local value of  $\Omega$  may differ from the universal value at a similar level.

We have assumed throughout that the additional scatter in the density–density scatterplots (over and above that due to the distance errors which scatter the POTENT densities) is due to other small unquantified errors in the POTENT density fields. As discussed in Section 4.4, the amount of additional scatter is comparable to our estimates of these systematic errors. However, it is also possible that spatial variations in the biasing relation between galaxies and mass may be large on scales of  $12h^{-1} \text{ Mpc}$ . For example, Cen & Ostriker (1993) investigated hydrodynamic simulations of the Cold Dark Matter cosmology and found on scales of  $10h^{-1} \text{ Mpc}$  a non-linear biasing relation which corresponds roughly to  $b_O \simeq 1.2 - 1.4$  in the range  $-0.5 < \delta < 1.0$ , in

good agreement with our results. The rms scatter in their biasing relation is about 0.23 in  $\delta_O$  at  $\delta_O = 0$ , comparable to the scatter of  $\sim 0.15$  which we would need to add in quadrature to the optical galaxy density to obtain good fits. If there are significant spatial variations in the efficiency of galaxy formation, then this adds an astrophysical source of scatter in the  $\delta - \delta_O$  plot which must be accounted for in the analysis. If this extra scatter is assigned to  $\delta_O$  then the slope of the regression changes to  $\beta_O \sim 1$ .

The current estimates of  $\Omega$  and  $b$  from large-scale structure are reviewed by Dekel (1994, section 8 and his table 1). In particular, the result for  $\beta_O$  found here is lower than the value  $\beta_I = 1.28_{-0.59}^{+0.75}$  (95 per cent confidence) found by DBY93, who compared an earlier realization of POTENT with the 1.9-Jy *IRAS* density field. A comparison between the 1.2-Jy *IRAS* density field and the new version of POTENT is in progress (D95d). If we allow for the fact that *IRAS* galaxies are less clustered (biased) than optical galaxies by a relative factor of  $\sim 1.3$  on the scales studied in this paper (Hudson 1993a; Peacock & Dodds 1994), then the different results for  $\beta$  lead to compatible values of  $\Omega$ .

Hudson (1994b) compared predicted peculiar velocities in linear theory from the optical density field smoothed with a 500 km s<sup>-1</sup> top-hat filter to observed peculiar velocities from the Mark II catalogue, and obtained the result  $\beta_O = 0.50 \pm 0.06$  (where the quoted errors are formal  $1\sigma$  random errors only). It seems at this early stage, while the various analyses are still in progress and the systematic effects are not fully understood, that velocity-velocity comparisons tend in general to yield somewhat lower estimates for  $\beta$  than the estimates based on density-density comparisons (e.g. Nusser & Davis, private communication; Willick et al., in preparation). However, the results are not at all incompatible when one allows for the systematic uncertainties in both determinations. A possible physical explanation for this difference in  $\beta$  is a variation in the biasing relation with scale or density.

The lower bounds on  $\Omega$  from cosmic flows independent of biasing (e.g. Nusser & Dekel 1993; Dekel & Rees 1994; see the review by Dekel 1994) are currently at the level of  $\Omega > 0.3$  with 99 per cent confidence, consistent with the theoretically favoured value of  $\Omega = 1$ . Other input of relevance include (i) constraints from the microwave background fluctuations, (ii) rms number fluctuations of optical and *IRAS* galaxies in top-hat spheres of radius  $8h^{-1}$  Mpc ( $\sigma_{8,O} \approx 0.95$ ,  $\sigma_{8,I} \approx 0.65$ ), and (iii) theoretical expectations for biasing based on first-generation simulations with gas dynamics. A choice of parameters that is consistent with the result of this paper and all the constraints above would have mass fluctuations at the level of  $\sigma_8 \approx 0.75$ , and linear biasing factors  $b_O \approx 1.3$  and  $b_I \approx 0.9$  for optical and *IRAS* galaxies respectively.

## ACKNOWLEDGMENTS

This research has been supported by PPARC through the rolling grant for Extragalactic Astronomy and Cosmology at Durham, the US-Israel Binational Science Foundation, and the Israel Science Foundation. MJH and AD acknowledge the hospitality of the Institut d'Astrophysique de Paris where part of this work was done.

## REFERENCES

- Aaranson M., Huchra J., Mould J., Schechter P. L., Tully R. B., 1982, *ApJ*, 258, 64
- Babul A., Weinberg D., Dekel A., Ostriker J. P., 1994, *ApJ*, 427, 1
- Bertschinger E., Dekel A., 1989, *ApJ* 336, L5
- Bertschinger E., Dekel A., Faber S. M., Dressler A., Burstein D., 1990, *ApJ*, 364, 370
- Burstein D., 1990, Mark II compilation of peculiar velocities, privately circulated
- Cen R., Ostriker J. P., 1993, *ApJ*, 417, 415
- Courteau S., 1992, PhD Thesis, University of California, Santa Cruz
- da Costa L. N., et al., 1988, *ApJ*, 327, 544
- da Costa L. N., Pellegrini P. S., Davis M., Meiksin A., Sargent W. L. W., Tonry J. L., 1991, *ApJS*, 75, 935
- Davis M., Huchra J., 1982, *ApJ*, 254, 437
- Dekel A., 1994, *ARA&A*, 32, 371
- Dekel A., Rees M., 1994, *ApJ*, 422, L1
- Dekel A., Bertschinger E., Faber S. M., 1990, *ApJ*, 364, 349 (DBF)
- Dekel A., Bertschinger E., Yahil A., Strauss M. A., Davis M., Huchra J. P., 1993, *ApJ*, 412, 1 (DBY93)
- Dressler A., 1991, *ApJS*, 75, 241
- Dressler A., Faber S., Burstein D., 1991, *ApJ*, 368, 54
- Faber S. M., Wegner G., Burstein D., Davies R. L., Dressler A., Lynden-Bell D., Terlevich R. J., 1989, *ApJS*, 69, 763
- Fairall A. P., Jones A., 1991, Southern Redshift Catalogue. Publ. Dept. Astron., Univ. Cape Town, No. 11
- Fisher K., 1992, PhD Thesis, University of California, Berkeley
- Giovanelli R., Haynes M. P., 1985, *AJ*, 90, 2445
- Giovanelli R., Haynes M. P., Myers S., Roth J., 1986, *AJ*, 92, 250
- Han M-S., 1991, PhD Thesis, California Institute of Technology
- Han M., Mould J. R., 1992, *ApJ*, 396, 453
- Huchra J. P., 1988, in van den Bergh S., Pritchet C. J., eds, ASP Conf. Ser. No. 4, The Extragalactic Distance Scale. Astronomical Society of the Pacific, San Francisco, p. 257
- Huchra J. P., 1990, ZCAT, privately circulated
- Huchra J., Davis M., Tonry J., Latham D., 1983, *ApJS*, 52, 89
- Hudson M. J., 1993a, *MNRAS*, 265, 43
- Hudson M. J., 1993b, *MNRAS*, 265, 72
- Hudson M. J., 1994a, *MNRAS*, 266, 468
- Hudson M. J., 1994b, *MNRAS*, 266, 475
- Hudson M. J., Lynden-Bell D., 1991, *MNRAS*, 252, 219
- Kaiser N., Efstathiou G., Ellis R., Frenk C., Lawrence A., Rowan-Robinson M., Saunders W., 1991, *MNRAS*, 252, 1
- Lauberts A., 1982, The ESO-Uppsala Survey of the ESO(B) Atlas. European Southern Observatory (ESO)
- Lucey J. R., Carter D., 1988, *MNRAS*, 235, 1177
- Lynden-Bell D., Lahav O., Burstein D., 1989, *MNRAS*, 241, 325
- Mathewson D. S., Ford V. L., Buchhorn M., 1992, *ApJS*, 81, 413
- Mould J. R., Stavely-Smith L., Schommer R. A., Bothun G. D., Jall P. J., 1991, *ApJ*, 383, 467
- Mould J. R., Akesson R. L., Bothun G. D., Han M-S., Huchra J. P., Roth J., Schommer R. A., 1993, *ApJ*, 409, 14
- Nilson P., 1973, Uppsala General Catalogue of Galaxies. Uppsala Astron. Obs. Ann., 6 (UGC)
- Nusser A., Dekel A., 1993, *ApJ*, 405, 437
- Nusser A., Dekel A., Bertschinger E., Blumenthal G. R., 1991, *ApJ*, 379, 6
- Peacock J. A., Dodds S. J., 1994, *MNRAS*, 267, 1020
- Peebles P. J. E., 1980, The Large Scale Structure of the Universe. Princeton Univ. Press, Princeton
- Shaya E. J., Tully R. B., Pierce M. J., 1992, *ApJ*, 391, 16
- Strauss M. A., 1989, PhD Thesis, University of California, Berkeley
- Strauss M. A., Davis M., Yahil A., Huchra J. P., 1990, *ApJ*, 361, 49

- Strauss M. A., Huchra J. P., Davis M., Yahil A., Fisher K., Tonry J., 1992, ApJS, 83, 29
- Tormen G., Burstein D. B., 1995, ApJS, in press.
- Willick J.A., 1991, PhD Thesis, University of California, Berkeley
- Willick J.A., 1994, ApJS, 92, 1
- Willick J. A., Courteau S., Faber S. M., Burstein D., Dekel A., 1995, ApJ, in press
- Yahil A., Strauss M. A., Davis M., Huchra J. P., 1991, ApJ, 372, 380